Available online at www.sciencedirect.com
SCIENCE DIRECT®
Computers and Structures 81 (2003) 2525–2538
Computers & Structures
www.elsevier.com/locate/compstruc

New layerwise theories and finite elements for efficient thermal analysis of hybrid structures

J. Noack [a], R. Rolfes [b,*], J. Tessmer [b]

[a] MTU Aero Engines, Dachauer Str. 656, Munich, Germany
[b] DLR, Institute of Structural Mechanics, Structural Analysis Section, Lilienthalplatz 7, 38108 Braunschweig, Germany

Received 4 April 2002; accepted 3 July 2003

Abstract

Hybrid structures, for example metallic multiwall thermal protection systems, sandwiches or hot structures, consist of layers with different thermal conductivity. In addition, radiation and convection can occur within these layers. Analysis of these internal heat transfer mechanisms and the design of hybrid structures require three-dimensional models leading to a high modelling effort. With a new layerwise theory for heat conduction of hybrid structures this effort can be drastically reduced. Hybrid structures are idealized as structures with homogeneous layers characterised by different thermal conductivities. For layers with internal radiation exchange and convection an equivalent thermal conductivity is assumed.

By means of two heat transfer equilibrium conditions the nodal degrees of freedom become independent of the number of layers. Two four-noded finite shell elements QUADLLT and QUADQLT based on the new theory have been developed. These 2D finite elements enable the calculation of three-dimensional temperature distributions within hybrid structures. Comparison with 3D analysis and test results shows good agreement.

Keywords: Thermal analysis; Finite elements; Hybrid structures; Composites

1. Introduction

Modern design of thermo-mechanically loaded aerospace structures often leads to hybrid structures consisting of multiple layers from different material. Thermal protection systems (TPS), hot structures with different layers, cryogenic tanks, carbon or glass fibre reinforced metal laminates (CARE, GLARE) and sandwich structures are examples of such structures (conf. Fig. 1). All three heat transfer mechanisms, i.e. heat conduction, radiation and convection, can occur within hybrid structures.

The present paper focuses on a fast thermal analysis method which is suitable for whole structures. Consequently, local effects like detailed temperature distributions within the clips of a hot structure or the honeycomb core sheets of a sandwich structure (conf. Fig. 1) are not of primary interest. Due to this and for the sake of a clear modelling method, all heat transfer mechanisms within the structure are combined to an equivalent heat conduction. As it can be seen for a honeycomb core (conf. Fig. 2), all three mechanisms of heat conduction, radiation and convection are presented within hybrid structures. Methods for homogenization to derive an equivalent conduction are described by Heemskerk et al. [1] and Chamis et al. [2]. Beside the theoretical methods of homogenization, effective conduction values will be measured by experimental methods on structural level which are in accordance with such defined equivalence conduction parameters. In general, the resulting multi-layered structure has layerwise different anisotropic and temperature dependent

* Corresponding author.
E-mail address: raimund.rolfes@dlr.de (R. Rolfes).

0045-7949/$ - see front matter © 2003 Elsevier Ltd. All rights reserved.
doi:10.1016/S0045-7949(03)00300-6

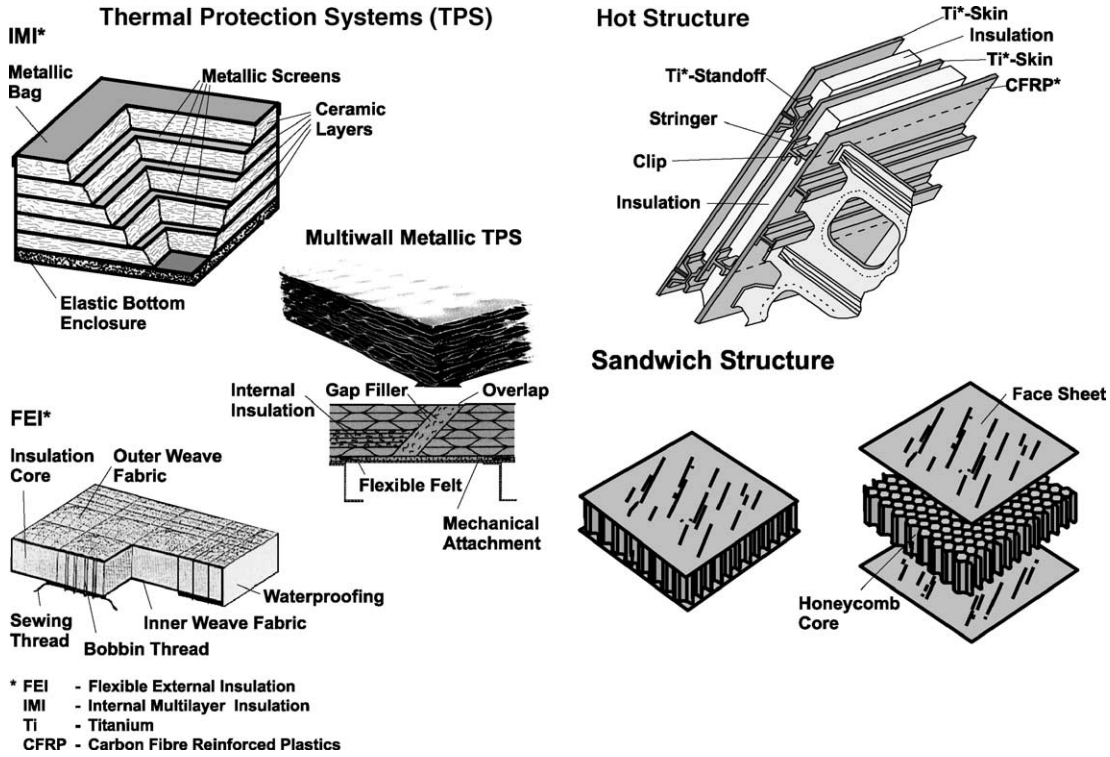

Fig. 1. Hybrid structures.

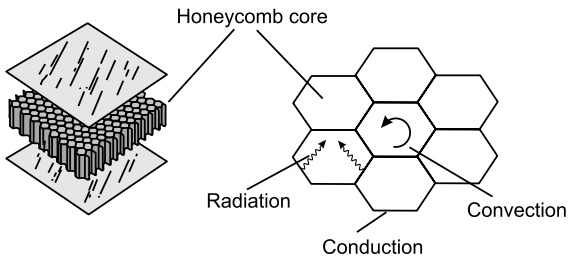

Fig. 2. Heat transfer mechanisms in honey comb core.

thermal conductivities, representing all relevant modes of heat transfer.

Thermal analysis of these structures can be carried out using the finite element method (FEM) or the finite difference method (FDM). MSC/NASTRAN, ANSYS or MARC are examples of commercial computer programmes based on the FEM. P/THERMAL, IDEAS-TMG, SINDA or ESATAN are using the FDM.

Practical experience shows that the FDM is especially well suited for problems, where radiation is the predominant heat transfer mechanism, e.g. in satellites. However, for problems, where heat conduction is of major concern, the FEM seems to be more appropriate to the authors. The choice of suitable shape functions, taking into account the anisotropic and heterogeneous conductivity, is easily manageable within the FEM and the combination of analytical pre-integration in thickness direction and numerical in-plane integration is readily formulated. Furthermore, reasonable skew and irregular meshes provide no remarkable difficulties for finite element formulations whereas for the FDM problems with uncertain results are reported in [3]. Additionally, the new formulation for hybrid composites can also build on thermal lamination theories (TLTs) for composites of constant thermal conductivity in thickness direction [4,5] which are already formulated using FEM. Another aspect comes into vision when regarding the interaction between thermal and stress analysis. Usually, thermal protection systems are neglected in the stress analysis and only the underlying thin-walled structure is taken into account. Equally, many sandwich and hot structures are thin walled. Therefore, the stress analysis is most frequently conducted by use of shell finite elements. Coupling a finite element based thermal analysis to those shell elements promises to be the generic and most suitable way, which leads to minimal coupling effort. A deeper discussion of advantages between FEM and FDM can be found in [6].

Using FEM a hybrid structure can be modeled using conventional three-dimensional heat conduction elements. Applying shell elements instead, would reduce

modeling and calculation effort and ease up temperature transference to the model for stress analysis. However, suitable lamination theories for hybrid structures are presently not available. For isotropic, axisymmetric problems Surana and Kalim [7] proposed a shell finite element with a linear approximation of the radial temperature distribution. Based on this work Surana and Phillips [8] developed a general shell element for thin-walled structures. That formulation uses temperatures and temperature gradients in transverse direction as nodal degrees of freedom. For composite structures Noor and Burton [9] proposed a predictor–corrector procedure. Within the predictor step, a linear temperature distribution in transverse direction is determined. Within the corrector step this distribution is improved by use of three-dimensional heat conduction equations. TLTs with linear and quadratic formulations for the transverse temperature distribution were proposed by Rolfes [4,5]. Based on these theories two quadrilateral finite shell elements (QUADTL for the linear and QUADQL for the quadratic theory) were developed and applied to linear and non-linear, steady-state and transient problems [10]. The interaction with stress analysis is outlined in [11,12]. Argyris et al. [13] used *Rolfes*' linear TLT and developed a triangular finite element for steady-state non-linear heat conduction.

For highly transient processes or in case of extremely concentrated thermal loads higher than quadratic approximations in transverse direction might be necessary. Surana and Orth [14] proposed an axial symmetric shell element with p-approximation in thickness direction. The element heat conduction matrix is calculated by a layerwise numerical integration procedure, where the computational effort increases with the number of layers.

For standard composites the thermal conductivity in thickness direction is constant, leading to $C^{(1)}$-continuity of temperatures. This, however, is not the case for hybrid structures. Therefore, the assumption of a $C^{(1)}$-continuous temperature distribution in thickness direction does not correspond with reality. However, a layerwise formulation can account for this aspect. Sipetov et al. [15] proposed a layerwise linear formulation. Unfortunately, they used unidirectional composites in their numerical examples; thus the full potential of the formulation could not be shown and additionally a non-linear formulation was not presented, leading to poor results for concentrated loads (see Section 5). Bose and Surana [16] developed an axisymmetric and three-dimensional curved shell finite element with a piecewise p-version approach for the analysis of heat conduction in thick composites. The number of nodal degrees of freedom increases with the number of layers and the order of the polynomial approximation.

This paper will present layerwise theories (linear and quadratic) which are applicable for hybrid composites with a layer independent number of nodal degrees. The outline is as follows. In Section 2 linear and quadratic layerwise theories (QLTs) are introduced where the number of functional degrees of freedom is independent of the number of layers. Finite shell elements based on the new formulations are developed within Section 3. Section 4 comprises coupling effects between structural parts having different stacking sequences (2D–2D coupling) as well as local effects (2D–3D coupling). The paper closes with numerical examples and conclusions.

2. New layerwise theories

The heat conduction can be described by *Fourier's law*

$$\mathbf{q} = -k(\operatorname{grad} T) \tag{1}$$

with temperature T, thermal conductivity k and heat flux vector $\mathbf{q}$. In anisotropic materials the thermal conductivity is defined by the second order tenser $\mathbf{K}$ which depends on the material orientation and Fourier's law must be rewritten as

$$\mathbf{q} = -\mathbf{K} \cdot (\operatorname{grad} T). \tag{2}$$

In the following, structures with a layerwise build-up are considered. The local laminate coordinate systems are chosen in a way that the x-axis and the y-axis lie within the layers plane and the z-axis is perpendicular to it. See also Fig. 6 for specific local coordinate definitions in thickness direction.

The following assumptions are necessary for the layerwise linear theory:

(1) Within each homogeneous layer k the heat conduction is described by a thermal conductivity tensor for monoclinic systems

$$\mathbf{K}^{(k)} = \begin{bmatrix} k_{xx}^{(k)} & k_{xy}^{(k)} & 0 \\ k_{yx}^{(k)} & k_{yy}^{(k)} & 0 \\ 0 & 0 & k_{zz}^{(k)} \end{bmatrix}. \tag{3}$$

(2) The material properties are independent of temperature.
(3) There is perfect thermal contact between all layers.
(4) No heat flux is generated inside the layers.

2.1. Linear layerwise theory

For the LLT a linear temperature distribution in transverse direction of a single layer k is assumed.

$$T^{(k)}(x,y,z) = T_0^{(k)}(x,y) + z_k \cdot T_{0,z}^{(k)}(x,y); \qquad -\frac{t_k}{2} \leqslant z_k \leqslant +\frac{t_k}{2}. \tag{4}$$

The functional degrees of freedom in Eq. (4) are the temperature of the layers middle surface $T_0^{(k)}(x,y)$ and its partial temperature gradient $T_{0,z}^{(k)}(x,y)$. If N is the number of layers then $2 \cdot N$ functional degrees of freedom occur. This is reduced to only two degrees of freedom by applying two heat transfer equilibrium conditions at each layer interface.

The first condition

$$T^{(k)}\left(\frac{t_k}{2}\right) = T^{(k+1)}\left(-\frac{t_{k+1}}{2}\right), \tag{5}$$

justified by assumption 3, demands continuity of the temperature at the layer interfaces.

The second condition reads

$$q_z^{(k)}\left(\frac{t_k}{2}\right) = q_z^{(k+1)}\left(-\frac{t_{k+1}}{2}\right). \tag{6}$$

It is physically justified by assumption 4 and ensures continuity of the transverse heat flux q_z. Together with Eq. (4), where the linear temperature distribution assures a layerwise constant heat flux q_z, follows then

$$q^{(k+1)} = q^{(k)} = \text{const.} \tag{7}$$

By applying Eqs. (2) and (3) follows

$$T_{0,z}^{(k+1)} = \frac{k_{zz}^{(k)}}{k_{zz}^{(k+1)}} T_{0,z}^{(k)}. \tag{8}$$

Introducing Eqs. (4) and (8) into (5) leads to

$$T_0^{(k+1)} = T_0^{(k)} + \frac{T_{0,z}^{(k)}}{2} \cdot \left(t_k + \frac{k_{zz}^{(k)}}{k_{zz}^{(k+1)}} t_{k+1}\right). \tag{9}$$

With Eqs. ((8) and (9)) the functional degrees of freedom of layer $k+1$ can be calculated from the values of the functional degrees of freedom of layer k.

Thus, if temperature and temperature gradient of one layer as well as the conductivities of all layers are known the complete transverse temperature distribution at line (x,y) can be determined step by step. An arbitrary layer is defined as reference layer b. With

$$s_k = \begin{cases} \frac{1}{2} \cdot \sum_{i=b}^{k-1} \left(\frac{t_i}{k_{zz}^{(i)}} + \frac{t_{i+1}}{k_{zz}^{(i+1)}}\right); & b < k \\ 0; & b = k \\ -\frac{1}{2} \cdot \sum_{i=k+1}^{b} \left(\frac{t_i}{k_{zz}^{(i)}} + \frac{t_{i-1}}{k_{zz}^{(i-1)}}\right); & b > k \end{cases} \tag{10}$$

and the transformation of the local coordinate z_k to the global coordinate z

$$z_k = z + d_k; \quad \bar{z}_k \leqslant z \leqslant \bar{z}_{k+1} \tag{11}$$

$$d_k = \begin{cases} -\frac{1}{2} \cdot \sum_{i=b}^{k-1} (t_i + t_{i+1}); & b < k \\ 0; & b = k \\ \frac{1}{2} \cdot \sum_{i=k+1}^{b} (t_i + t_{i-1}); & b > k \end{cases} \tag{12}$$

the complete temperature distribution is determined by

$$T(x,y,z) = T_0^{(b)}(x,y) + Z_L(z) \cdot T_{0,z}^{(b)}(x,y), \tag{13}$$

with

$$Z_L(z) = k_{zz}^{(b)} \cdot \left(s_k + \frac{1}{k_{zz}^{(k)}}(z + d_k)\right), \quad k = \text{layer-index}, \tag{14}$$

where $T_0^{(b)}$ and $T_{0,z}^{(b)}$ are the only functional degrees of freedom remaining.

2.2. Quadratic layerwise theory

The previous section has shown a linear theory which is especially suitable for steady state thermal problems and uniform boundary conditions. For transient problems and hot spot loads the temperature distribution in transverse direction is non-linear. For these cases the quadratic approach

$$T^{(k)}(x,y,z) = T_0^{(k)}(x,y) + z_k \cdot T_{0,z}^{(k)}(x,y) + \frac{z_k^2}{2} \cdot T_{0,zz}^{(k)}(x,y); \quad -\frac{t_k}{2} \leqslant z_k \leqslant +\frac{t_k}{2} \tag{15}$$

is suggested. It allows for variation of the heat flux in transverse direction. Thus, Eq. (7) does not hold anymore. Initially, this theory leads to 3N functional degrees of freedom. Reducing the number to three requires an additional interface condition as compared to the linear theory. The third heat transfer equilibrium is chosen to be.

$$q_{z,z}^{(k)} = q_{z,z}^{(k+1)} = \text{const.} \tag{16}$$

While this seems to be mathematically stringent, there is physically no justification for this interface condition. Alternatively, it could also be assumed

$$T_{,zz}^{(k)} = T_{,zz}^{(k+1)} = \text{const.}, \tag{17}$$

which means that the curvature of the transverse temperature distribution is constant with z. However, numerical examples (conf. Section 5) have shown that Eq. (16) generally provides very reasonable results.

For the quadratic theory the three heat transfer equilibrium conditions provide

$$T_{0,zz}^{(k+1)} = \frac{k_{zz}^{(k)}}{k_{zz}^{(k+1)}} T_{0,zz}^{(k)}, \tag{18}$$

$$T_{0,z}^{(k+1)} = \frac{k_{zz}^{(k)}}{k_{zz}^{(k+1)}} T_{0,z}^{(k)} + T_{0,zz}^{(k)} \frac{k_{zz}^{(k)}}{2k_{zz}^{(k+1)}} (t_k + t_{k+1}), \tag{19}$$

$$T_0^{(k+1)} = T_0^{(k)} + \frac{T_{0,z}^{(k)}}{2}\left(t_k + \frac{k_{zz}^{(k)} \cdot t_{k+1}}{k_{zz}^{(k+1)}}\right) + T_{0,zz}^{(k)} k_{zz}^{(k)} \left[\frac{1}{2k_{zz}^{(k+1)}}(t_k + t_{k+1}) \cdot \left(\frac{t_{k+1}}{2}\right) + \frac{1}{8}\left(\frac{t_k^2}{k_{zz}^{(k)}} - \frac{t_{k+1}^2}{k_{zz}^{(k+1)}}\right)\right]. \quad (20)$$

Eq. (18) directly evolves from Eq. (16), Eq. (19) then follows with Eq. (6), and Eq. (20) with Eq. (5). The complete temperature distribution can now be described by

$$T(x,y,z) = T_0^{(b)}(x,y) + Z_L(z) \cdot T_{0,z}^{(b)}(x,y) + \frac{1}{2} Z_Q(z) \cdot T_{0,zz}^{(b)}(x,y), \quad (21)$$

with $Z_L(z)$ from Eq. (14) and

$$Z_Q(z) = 2(g_k + h_k) + f_k(t_k v_k + 2d_k + 2z) + \frac{k_{zz}^{(b)}}{k_{zz}^{(k)}}(d_k + z)^2, \quad k = \text{layer-index}, \quad (22)$$

where

$$v_k = \begin{cases} 1; & b < k \\ 0; & b = k \\ -1; & b > k \end{cases}, \quad (23)$$

$$f_k = \begin{cases} \frac{k_{zz}^{(b)}}{2k_{zz}^{(k)}} \sum_{i=b}^{k-1}(t_i + t_{i+1}); & b < k \\ 0; & b = k \\ -\frac{k_{zz}^{(b)}}{2k_{zz}^{(k)}} \sum_{i=b}^{k+1}(t_i + t_{i-1}); & b > k \end{cases}, \quad (24)$$

$$h_k = \begin{cases} \sum_{i=b+1}^{k-1}(t_i \cdot f_i); & b+1 < k \\ 0; & \text{for all other } k \\ -\sum_{i=b-1}^{k+1}(t_i \cdot f_i); & b-1 > k \end{cases}, \quad (25)$$

$$g_k = \frac{1}{8} \cdot \left(t_b^2 - \frac{t_k^2 \cdot k_{zz}^{(b)}}{k_{zz}^{(k)}}\right). \quad (26)$$

The analogy to thermal laminate theories for standard laminates Rolfes [4,5] is clearly visible since the structure of the equations remains the same. All different material properties in z-direction are included in the generalized thickness coordinates $Z^L(z)$ and $Z_Q(z)$, interpreting them as geometrical stretching or compression of the reference material. Fig. 3 shows principle temperature distributions as described by the linear and the quadratic layerwise theory.

3. Finite element formulation

Subsequently, two four-noded finite shell elements will be developed based on the new layerwise theories. The weak formulation of the general heat conduction equation over the domain Ω which is bounded by Γ reads

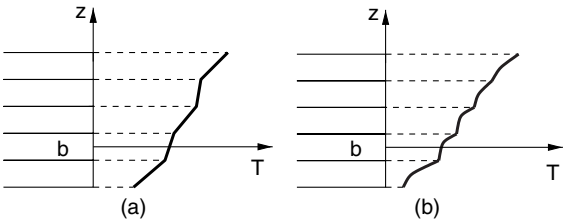

Fig. 3. Temperature distribution in transverse direction for layerwise theories.

$$\int_\Omega (\operatorname{grad} \mathbf{v})^{\mathrm{T}} \mathbf{K} \operatorname{grad} \mathbf{T} \, \mathrm{d}\Omega + \int_\Gamma \mathbf{q}^{\mathrm{T}} \mathbf{n} \mathbf{v} \, \mathrm{d}\Gamma = 0, \quad (27)$$

where $\mathbf{v}$ is the test function and $\mathbf{n}$ is the unit normal vector on the domain boundary. Free convection q_c and prescribed heat flux $\bar{q}$ boundary conditions according to

$$\mathbf{q}^{\mathrm{T}} \mathbf{n} = q_c + \bar{q}, \quad (28)$$

with

$$q_c = \alpha_c (T_W - T_\infty) \quad (29)$$

are considered. α_c is the convection coefficient, T_W and T_∞ are wall and ambient temperature, respectively.

Adopting a matrix formulation and following Eqs. (13) and (21) the temperature distribution of a single layer can be expressed as

$$\mathbf{T}^k(x,y,z) = \mathbf{R} \cdot \boldsymbol{\varrho}, \quad (30)$$

where the coefficient vector reads

$$\mathbf{R}_{\mathrm{L}} = \left[1 \quad 0 \quad 0 \quad k_{zz}^{(b)} \cdot \left(s_k + \tfrac{1}{k_{zz}^{(k)}} \cdot (z + d_k)\right) \quad 0 \quad 0\right], \quad (31)$$

or

$$\mathbf{R}_{\mathrm{Q}} = \left[1 \quad 0 \quad 0 \quad k_{zz}^{(b)} \cdot \left(s_k + \tfrac{1}{k_{zz}^{(k)}} \cdot (z + d_k)\right) \quad 0 \quad 0 \quad \tilde{r} \quad 0 \quad 0\right], \quad (32)$$

with

$$\tilde{r} = g_k + h_k + \frac{f_k t_k v_k}{2} + f_k(z + d_k) + \frac{k_{zz}^{(b)}(z + d_k)^2}{2k_{zz}^{(k)}}, \quad (33)$$

and $\boldsymbol{\varrho}$ is the vector of the functional degrees of freedom

$$\boldsymbol{\varrho}_L = [\, T_0^{(b)} \quad T_{0,x}^{(b)} \quad T_{0,y}^{(b)} \quad T_{0,z}^{(b)} \quad T_{0,zx}^{(b)} \quad T_{0,zy}^{(b)} \,]^{\mathrm{T}}, \quad (34)$$

$$\boldsymbol{\varrho}_Q = [\, T_0^{(b)} \quad T_{0,x}^{(b)} \quad T_{0,y}^{(b)} \quad T_{0,z}^{(b)} \quad T_{0,zx}^{(b)} \quad T_{0,zy}^{(b)} \quad T_{0,zz}^{(b)} \quad T_{0,zzx}^{(b)} \quad T_{0,zzy}^{(b)} \,]^{\mathrm{T}}. \quad (35)$$

The indices L and Q apply to the linear and the quadratic layerwise theory, respectively.

Consequently, the temperature gradient can be formulated as

$$\operatorname{grad}\mathbf{T} = \mathbf{S}\cdot\boldsymbol{\varrho}, \tag{36}$$

where S is the coefficient matrix

$$\mathbf{S}_{\mathrm{L}} = \begin{bmatrix} 0 & 1 & 0 & 0 & \tilde{s}_1 & 0 \\ 0 & 0 & 1 & 0 & 0 & \tilde{s}_1 \\ 0 & 0 & 0 & \frac{k_{zz}^{(b)}}{k_{zz}^{(k)}} & 0 & 0 \end{bmatrix}, \tag{37}$$

or

$$\mathbf{S}_{\mathrm{Q}} = \begin{bmatrix} 0 & 1 & 0 & 0 & \tilde{s}_1 & 0 & 0 & \tilde{r} & 0 \\ 0 & 0 & 1 & 0 & 0 & \tilde{s}_1 & 0 & 0 & \tilde{r} \\ 0 & 0 & 0 & \frac{k_{zz}^{(b)}}{k_{zz}^{(k)}} & 0 & 0 & \tilde{s}_2 & 0 & 0 \end{bmatrix}. \tag{38}$$

The value for $\tilde{s}_1$ and $\tilde{s}_2$ are defined as

$$\tilde{s}_1 = k_{zz}^{(b)} s_k + \frac{k_{zz}^{(b)}}{k_{zz}^{(k)}}\cdot(z+d_k), \tag{39}$$

and

$$\tilde{s}_2 = f_k + \frac{k_{zz}^{(b)}(z+d_k)}{k_{zz}^{(k)}}. \tag{40}$$

Matrices $\mathbf{S}_{\mathrm{L}}$ and $\mathbf{S}_{\mathrm{Q}}$ are found by partial derivation of (13) and (21).

The test functions $\mathbf{v}$ are treated analogous to the temperature. This results in

$$\mathbf{v} = \mathbf{R}\cdot\boldsymbol{\eta}, \tag{41}$$

and

$$\operatorname{grad}\mathbf{v} = \mathbf{S}\cdot\boldsymbol{\eta}, \tag{42}$$

where $\boldsymbol{\eta}$ are the test functions for the functional degrees of freedom. Introducing Eqs. (36), (41) and (42) into Eq. (27) yields

$$\int_A \boldsymbol{\eta}^{\mathrm{T}} \int_z \mathbf{S}^{\mathrm{T}}\mathbf{K}\mathbf{S}\,\mathrm{d}z\boldsymbol{\varrho}\,\mathrm{d}A + \int_\Gamma \mathbf{q}^{\mathrm{T}}\mathbf{n}\mathbf{R}\boldsymbol{\eta}\,\mathrm{d}\Gamma = 0. \tag{43}$$

It should be noted that the integration in thickness direction is independent of the finite element formulation and can be carried out analytically. This leads to

$$\overline{\mathbf{K}} = \int_{\mathbf{z}} \mathbf{S}^{\mathrm{T}}\mathbf{K}\mathbf{S}\,\mathrm{d}\mathbf{z}, \tag{44}$$

with

$$\overline{\mathbf{K}}_{\mathrm{L}} = \begin{bmatrix} 0 & 0 & 0 & 0 & 0 & 0 \\ 0 & A_{xx} & A_{xy} & 0 & B_{xx} & B_{xy} \\ 0 & A_{xy} & A_{yy} & 0 & B_{xy} & B_{yy} \\ 0 & 0 & 0 & A_{zz} & 0 & 0 \\ 0 & B_{xx} & B_{xy} & 0 & C_{xx} & C_{xy} \\ 0 & B_{xy} & B_{yy} & 0 & C_{xy} & C_{yy} \end{bmatrix}, \tag{45}$$

and

$$\overline{\mathbf{K}}_{\mathrm{Q}} = \begin{bmatrix} 0 & 0 & 0 & 0 & 0 & 0 & 0 & 0 & 0 \\ 0 & A_{xx} & A_{xy} & 0 & B_{xx} & B_{xy} & 0 & F_{xx} & F_{xy} \\ 0 & A_{xy} & A_{yy} & 0 & B_{xy} & B_{yy} & 0 & F_{xy} & F_{yy} \\ 0 & 0 & 0 & A_{zz} & 0 & 0 & B_{zz} & 0 & 0 \\ 0 & B_{xx} & B_{xy} & 0 & C_{xx} & C_{xy} & 0 & G_{xx} & G_{xy} \\ 0 & B_{xy} & B_{yy} & 0 & C_{xy} & C_{yy} & 0 & G_{xy} & G_{yy} \\ 0 & 0 & 0 & B_{zz} & 0 & 0 & C_{zz} & 0 & 0 \\ 0 & F_{xx} & F_{xy} & 0 & G_{xx} & G_{xy} & 0 & H_{xx} & H_{xy} \\ 0 & F_{xy} & F_{yy} & 0 & G_{xy} & G_{yy} & 0 & H_{xy} & H_{yy} \end{bmatrix}. \tag{46}$$

The procedure to derive all coefficients in $\overline{\mathbf{K}}_{\mathrm{L}}$ and $\overline{\mathbf{K}}_{\mathrm{Q}}$ is straightforward and can be conducted without any problem. If desired, they can be found explicitly in [17].

The finite element approximation of the functional degrees of freedom can be expressed as

$$\boldsymbol{\varrho} = \mathbf{N}\boldsymbol{\vartheta}, \tag{47}$$

where bilinear shape functions for quadrilateral elements are entailed in $\mathbf{N}$, and $\boldsymbol{\vartheta}$ comprises the nodal degrees of freedom (conf. Fig. 4). These are

$$\boldsymbol{\vartheta}_{\mathrm{L}} = [\,T_0^1 \quad T_{0,z}^1 \quad T_0^2 \quad T_{0,z}^2 \quad T_0^3 \quad T_{0,z}^3 \quad T_0^4 \quad T_{0,z}^4\,]^{\mathrm{T}} \tag{48}$$

and

$$\boldsymbol{\vartheta}_{\mathrm{Q}} = [\,T_0^1 \quad T_{0,z}^1 \quad T_{0,zz}^1 \quad T_0^2 \quad T_{0,z}^2 \quad T_{0,zz}^2 \quad \cdots \quad T_0^4 \quad T_{0,z}^4 \quad T_{0,zz}^4\,]^{\mathrm{T}} \tag{49}$$

for the linear theory (element QUADLLT) and the quadratic theory (element QUADQLT), respectively.

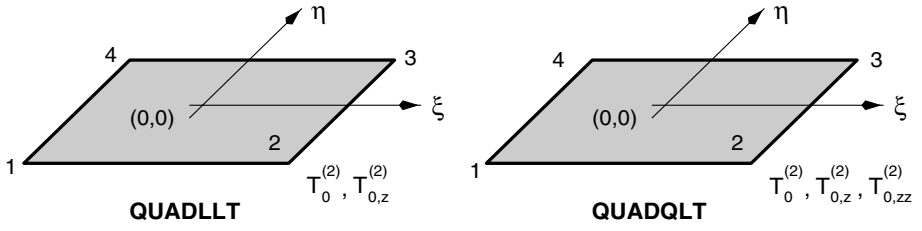

Fig. 4. Four-noded elements QUADLLT and QUADQLT with local coordinate system.

An isoparametric element concept is chosen. Applying Galerkin's method and introducing Eqs. (44) and (47) into Eq. (43) yields

$$\int_A \mathbf{N}^{\mathrm{T}}\overline{\mathbf{K}}\mathbf{N}\vartheta \,\mathrm{d}A + \int_\Gamma \mathbf{q}^{\mathrm{T}}\mathbf{n}\mathbf{N}^{\mathrm{T}}\mathbf{R}^{\mathrm{T}}\,\mathrm{d}\Gamma = 0. \tag{50}$$

The integral over Γ must be evaluated at the element surfaces and edges. The contribution of the edges is very efficiently taken into account by special rod elements (conf. Fig. 5), the formulation of which is straightforward [17].

4. Coupling of elements with different stacking sequence

In many practical problems the hybrid stacking (conf. Fig. 6) is not uniform throughout the whole structure. In that case junction areas are present which can be categorized as follows

1. Junctions of areas which both can be modelled by QUADLLT or QUADQLT elements but have different thickness and/or different stacking sequence (denoted as 2D–2D coupling, conf. Fig. 7).
2. Junctions of QUADLLT or QUADQLT elements with areas that must be modelled with 3D-elements (denoted as 2D–3D coupling).

Subsequently, the 2D–2D coupling is discussed, whereas 2D–3D coupling will be subject of future investigations. By means of a small example it is shown that coupling without the right strategy leads to erroneous results. A plate is considered under uniform heat flux at the top surface ($q = 200$ W/m^2) and convection boundary condition at the bottom surface ($\alpha_c = 14.5$ W/m^2, $T_\infty = 21$ °C). One-dimensional heat transfer occurs in transverse direction of the plate. Three different stacking sequences are investigated as depicted in Fig. 8. The material data are shown in Table 1. Mat 1 might be aluminium and Mat 2 might be some composite material.

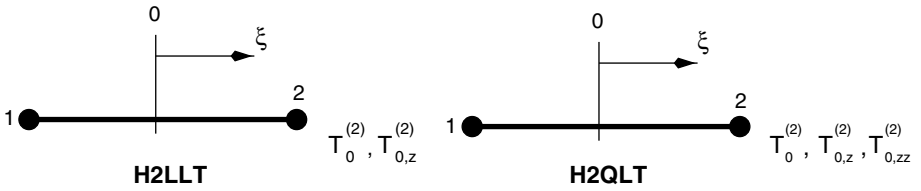

Fig. 5. Two-noded rod elements H2LLT and H2QLT.

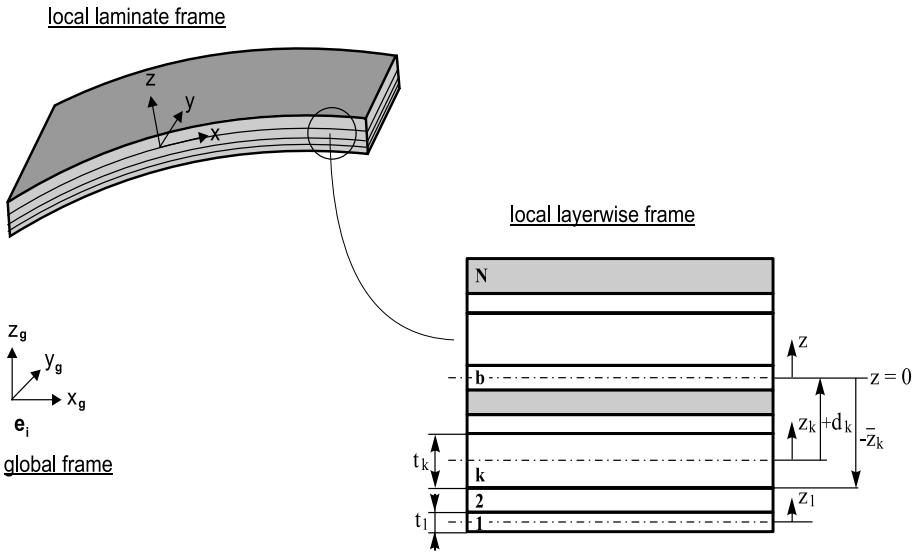

Fig. 6. Layered design of a hybrid structure.

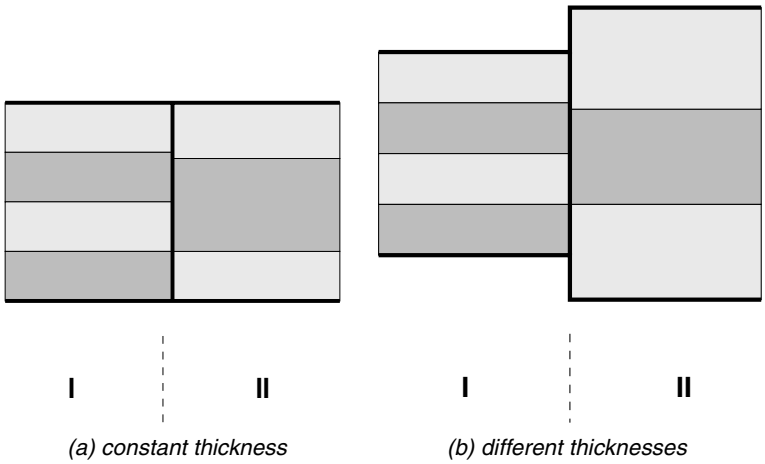

Fig. 7. 2D–2D coupling.

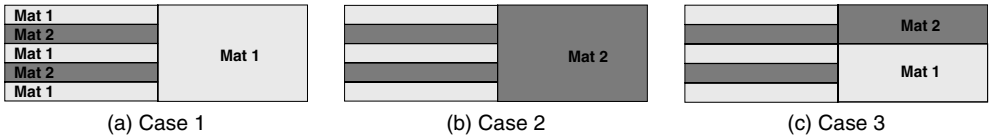

Fig. 8. Stacking sequences for demonstration problem. Mat 1: high conductivity, Mat 2: low conductivity.

Table 1
Heat conduction coefficients for the material

Material description	k_{xx} [W/m K]	k_{yy} [W/m K]	k_{zz} [W/m K]
Mat 1	254.0	254.0	254.0
Mat 2	26.8	0.96	0.96

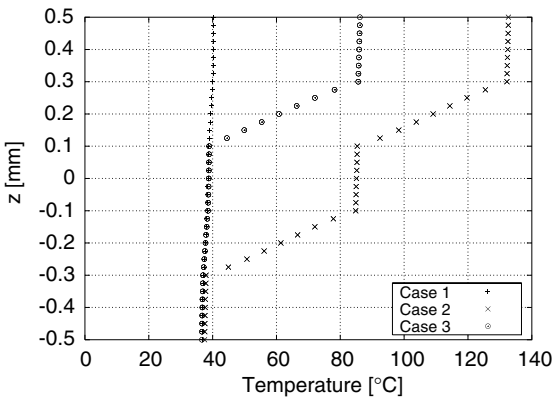

Fig. 9. Temperature distribution in transverse direction of the demonstration problem.

All cases were modelled using 3D eight-noded elements of MSC/NASTRAN. Fig. 9 shows the results at the junction of different stacking sequences. For case 2 the temperature distribution is dominated by the stacking sequence of the left side since the conductivity of the right side is small. In contrast to case 2 the temperature distribution for case 1 is extremely influenced by the high conductivity of the right side. Case 3, which is somewhere between the two extreme cases 1 and 2, underlines that the main heat path always leads through the material with higher conductivity. Multiple changes of the path from one side of the junction area to the other can occur. Fig. 10 shows the mesh discretization ($50\times50\times1$) and fringe plots for all three cases. Furthermore, the 3D analyses revealed that the temperature field within both regions is only affected very locally by the connection. When using the two-dimensional elements QUADLLT or QUADQLT for modelling such a connection point, usually all nodal degrees of freedom (two respectively three) at the connection point are equated. However, this does not provide a continuous temperature field over the whole cross section at the connection point since only the temperature and its derivatives at the reference plane are regarded. Calculating the full transverse temperature distribution from the equated degrees of freedom (conf. Eq. (11) resp. 16) results in different temperature profiles for the two regions. Furthermore, equating all functional degrees of freedom leads to erroneous results even in some distance from the connection point.

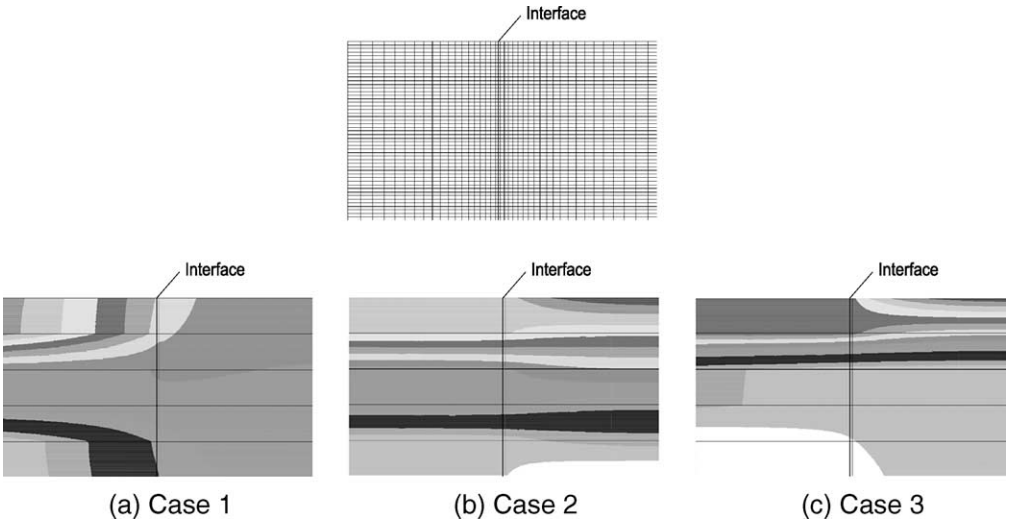

Fig. 10. Mesh discretization and fringe plots for demonstration problem.

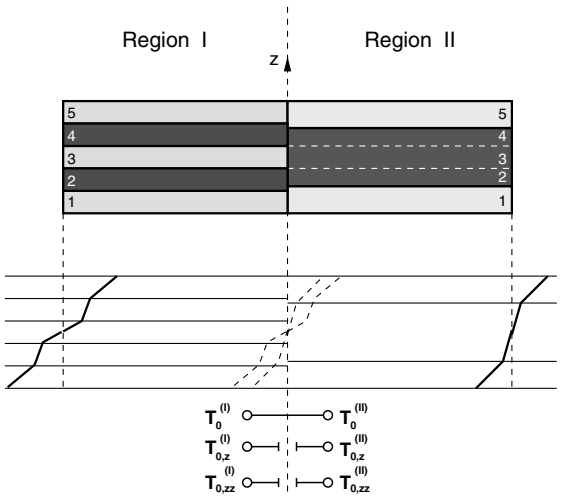

Fig. 11. Temperature distributions after disconnecting of the nodal degrees of freedom $T_{0,z}$ and $T_{0,zz}$.

Therefore, only the temperature of the reference plane is coupled and the higher degrees of freedom remain uncoupled. This provides good results at the surrounding nodes but still leads to two different distributions at the connection point (conf. Fig. 11). These are evened out by applying the weighting function

$$\overline{T}(z) = \frac{c_1\overline{T}_{|}(z) + c_2\overline{T}_{\|}(z)}{c_1 + c_2}, \quad c_1 = k_{zz,|}^{(k)}, \quad c_2 = k_{zz,\|}^{(k)}. \tag{51}$$

By choosing the heat conduction parameters as weighing components it is regarded that the better conducting material dominates the temperature field at the junction interface. Also, the formula ensures $\overline{T}(z=0) = \overline{T}_{|}(z=0) = \overline{T}_{\|}(z=0)$ at the reference surface.

A small example (Fig. 12) shows the application of this coupling method. The dimensions of both regions are $a = b = 1$ m. On the top of both regions acts an uniform heat flux of $q = 60$ W/m^2. At the bottom side free convection with $T_\infty = 21$ °C and $\alpha_c = 14.5$ W/m^2 K is assumed. Two different stacking sequences (Table 2) are investigated. The properties are given in Table 3. The model was analysed twice, firstly by use of QUADLLT and secondly by applying a three-dimensional model (HEX8 elements of MSC/NASTRAN). For the second case the HEX8-mesh with properties indicated and the thermal field fringe plot are plotted in Fig. 13. Fig. 14 shows the temperature distribution at the connection for case 1. The temperature distribution for region 1 provides wrong surface temperatures. The correction using Eq. (51) leads to a very good matching of the 3D result. Fig. 15 represents the results for case 2 with different thickness of region 1 and 2. Again, the weighting function provides excellent results.

5. Numerical examples

Three examples were analysed using the formulation presented. The first example, a cryo tank structure, is a typical hot structure. Fig. 16 shows the layered design of the cryo tank. Tests with heating by infrared radiators from one side and cooling the opposite side by liquid nitrogen were performed in the thermo-mechanical test facility TERMEX-B [18]. For the analysis a square sector of the tank was chosen. Due to a homogeneous in-plane temperature field, with gradients only in

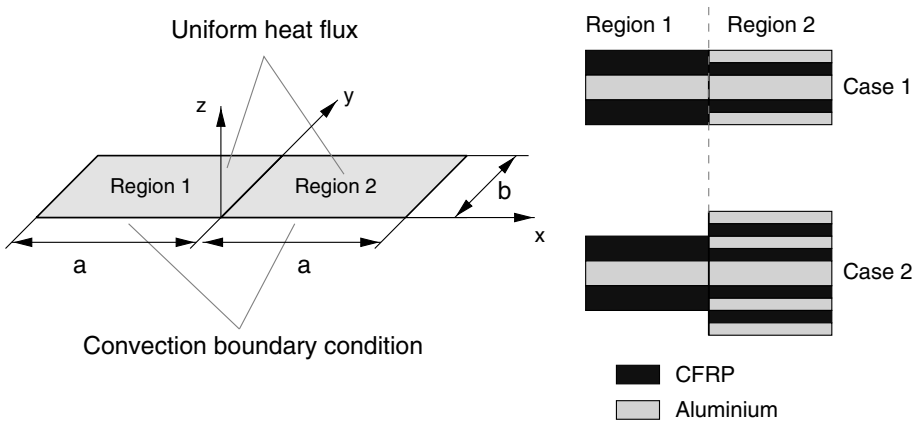

Fig. 12. Examples for 2D–2D coupling.

Table 2
Stacking sequences for examples of 2D–2D coupling

Layer	Region 1		Region 2 (case 1)		Region 2 (case 2)	
	Thickness [m]	Material	Thickness [m]	Material	Thickness [m]	Material
1	0.1	CFRP	0.05	Alu	0.05	Alu
2	0.025	Alu	0.05	CFRP	0,05	CFRP
3	0.05	Alu	0.025	Alu	0.05	Alu
4	0.025	Alu	0.05	Alu	0.05	CFRP
5	0.1	CFRP	0.025	Alu	0.025	CFRP
6			0.05	CFRP	0.05	Alu
7			0.05	Alu	0.025	CFRP
8					0.05	CFRP
9					0.05	Alu
10					0.05	CFRP
11					0.05	Alu

Table 3
Material properties for examples of 2D–2D coupling

Material	k_{xx} [W/m K]	k_{yy} [W/m K]	k_{zz} [W/m K]
Aluminium (Alu)	254.0	254.0	254.0
CFRP	28.6	0.96	0.96

thickness direction, the finite element analysis was performed using a 1×1 in-plane discretization. Out of plane, just one QUADLLT-element was used whereas 36 HEXA-elements were necessary for the 3D-analysis with MSC/NASTRAN. The material data are given in Table 4. Fig. 17 compares test results with 3D and QUADLLT calculations. Both numerical analyses lead to the same transverse temperature distribution. Uncertain thermal conductivities for the air and FEI layers lead to small difference between test and numerical results. This example shows the efficiency of the element for steady-state analyses with uniform loads. The expected layerwise linear temperature distribution is approximated very well.

The second and third example are both layered plates which are subjected to a locally concentrated heat flux (conf. Fig. 18). One of those is a sandwich construction whereas the other one consists of the hybrid composite CARE. In contrast to the first example, where the heat flow was mainly one-dimensional, the concentrated load causes three dimensional heat flow below the load. Consequently, the temperature distribution in thickness direction at point P can be layerwise non-linear. The geometrical dimensions were $a = 0.04$ m and $b = 0.01$ m. Along the edges and at the lower surface convection with $\alpha_c = 30$ W/m^{2}K and $T_\infty = 0$ °C was applied, at the upper surface adiabatic conditions were assumed outside the heat flux of $q = 100$ kW/m^2. The in-plane discretization is shown in Fig. 19.

CARE is a hybrid laminate made up from aluminium and CFRP layers. Stacking sequence and anisotropic conductivities are given in Table 5. The steady state

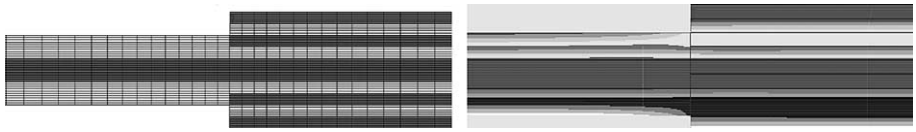

Fig. 13. HEX-8 mesh with indicated properties and thermal field for case 2 of 2D–2D coupling.

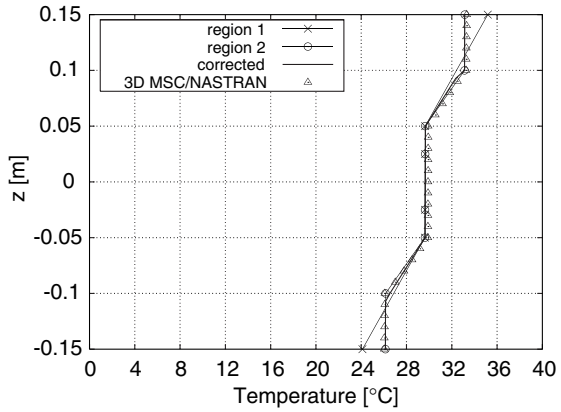

Fig. 14. Temperature distribution for Case 1 of the 2D–2D coupling.

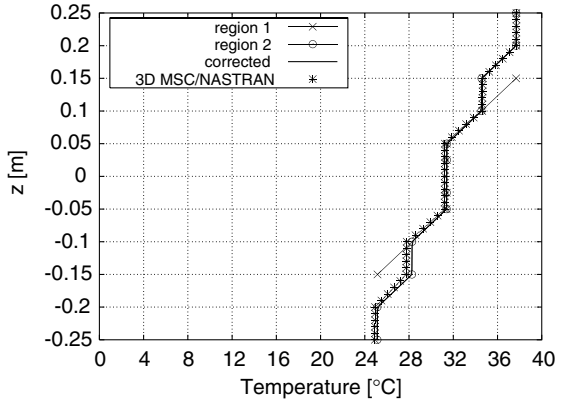

Fig. 15. Temperature distribution for Case 2 of the 2D–2D coupling.

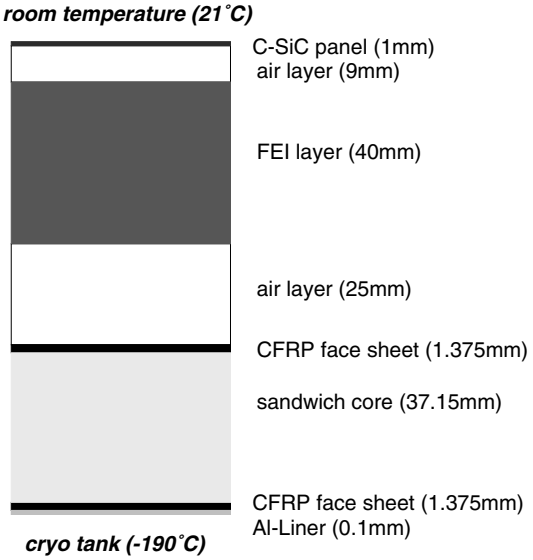

Fig. 16. Layered design of a cryo tank structure.

Table 4
Thermal conductivities of cryo tank structure

Material	k_{xx} [W/m K]	k_{yy} [W/m K]	k_{zz} [W/m K]
Al-liner	235.0	235.0	235.0
UD layer (CFRP)	26.208	0.96	0.96
Rohacell 71 WF	0.01	0.01	0.004
Air (at room temperature)	0.02	0.02	0.02
FEI-isolation	0.063	0.063	0.014
C–SiC panel	22.0	22.0	22.0

temperature distribution at point P is depicted in Fig. 20. It shows a comparison of both new elements with a full 3D analysis using HEXA elements of MSC.NASTRAN. The approximation of QUADLLT is already satisfactory, excellent results are provided by QUADQLT.

The sandwich shown in Fig. 21 has two facings with three layers each and a honeycomb core. This construction and the homogenized properties of the core were taken from Heemskerk et al. [1]. The conductivities are given in Table 6. Again the new elements are compared with a numerical 3D solution (conf. Fig. 22). Due to its high conductivity there is nearly no temperature gradient within the facings whereas a significant nonlinear temperature drop occurs in the core. It is clearly visible that QUADQLT is very well capable of describing this phenomenon whereas QUADLLT shows slight deviations. This example also describes the quality of convergence which is reached by the new element formulation. Since the in-plane formulation is the same (standard bi-linear shape functions) for all used finite elements, no difference of convergence behaviour is expected with respect to the in-plane discretization. Fig. 23

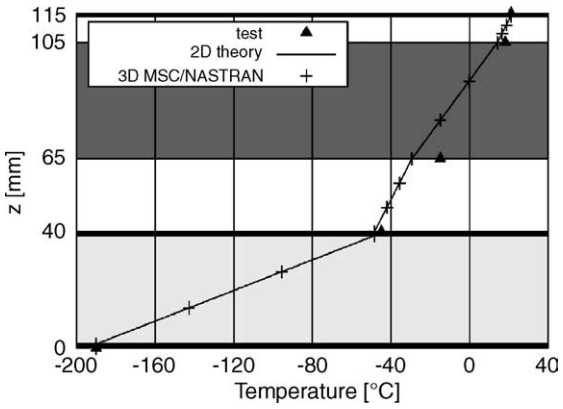

Fig. 17. Results of the cryo tank analysis.

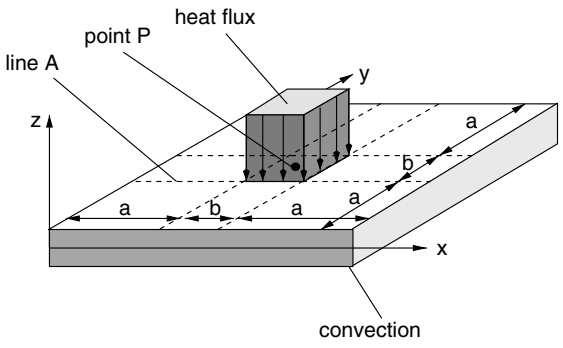

Fig. 18. In-plane discretization of plate with concentrated heat load.

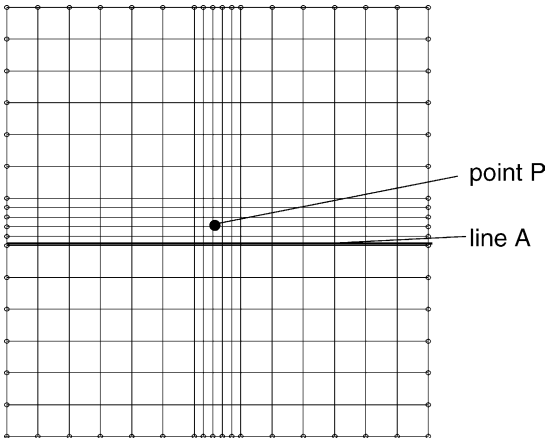

Fig. 19. Example dimensions and boundary conditions.

shows the in-plane temperature distribution of the upper side of the sandwich plate along line A (conf. Fig. 18). It shows no difference with the same discretization in-plane. Nevertheless, convergence towards the 3D-reference solution is seen in thickness direction from the linear to the quadratic layerwise theory (conf. Fig. 22). As it is self-saying that for the new 2D elements only one element can be taken in thickness direction, the order of the layerwise function space is important for a proper result.

It should be kept in mind that a strongly concentrated heat flux is a rather tough test for the elements. In many applications the thermal loading will be much more uniform and the temperature distribution can be kept properly already by the linear element.

Table 5
Construction and thermal conductivities of CARE plate

Layer	Thickness [mm]	Material	
1	0.3	Aluminum	
2	0.5	CFRP $[0°, 90°]_S$	
3	0.3	Aluminum	
4	0.5	CFRP $[0°, 90°]_S$	
5	0.3	Aluminum	
Material	k_{xx} [W/m K]	k_{yy} [W/m K]	k_{zz} [W/m K]
UD-layer (CFRP)	26.208	0.96	0.96
Aluminum	235.0	235.0	235.0

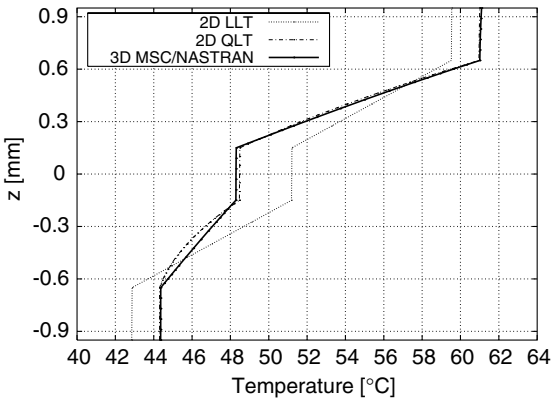

Fig. 20. Transverse temperature distribution at point P ($x = y = 44.0$ mm) of CARE plate.

6. Conclusion

In the present paper a linear and a quadratic layerwise theory for heat conduction of hybrid structures was developed. In contrast to the TLT [4,5] the thermal conductivity in transverse direction can be different from layer to layer. With two heat transfer equilibrium equations it was possible to reduce the number of de-

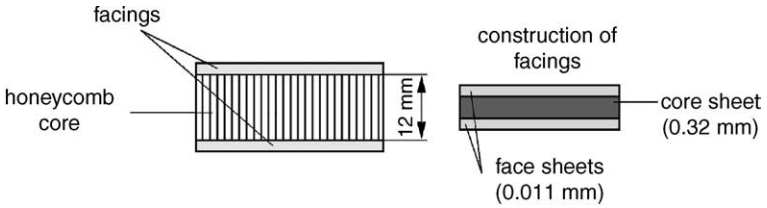

Fig. 21. Aufbau der Sandwich plate.

Table 6
Thermal conductivities of sandwich plate

Material	k_{xx} [W/m K]	k_{yy} [W/m K]	k_{zz} [W/m K]
Honeycomb core (al. 3003)	0.96	0.58	1.95
Core sheet (alu)	240.0	240.0	240.0
Face sheet (al. 2024T6)	150.0	150.0	150.0

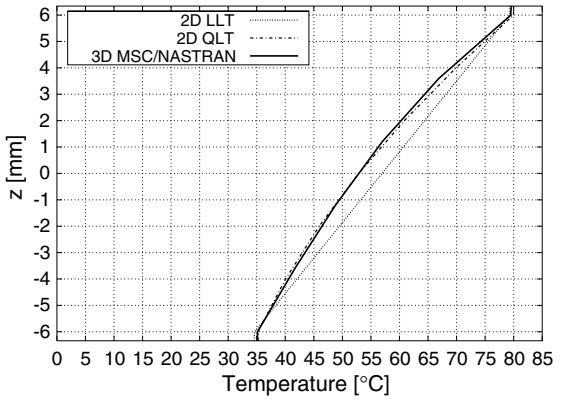

Fig. 22. Transverse temperature distribution at point P ($x = y = 44.0$ mm) of sandwich plate.

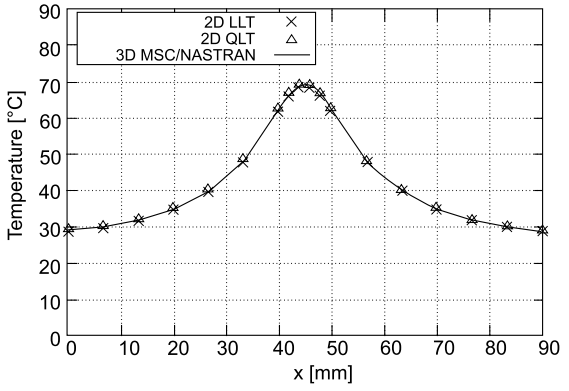

Fig. 23. Temperature on top of sandwich plate along line A.

grees of freedom and make it independent of the number of layers.

Based on these layerwise theories new finite shell elements for the analysis of the three-dimensional temperature distribution of hybrid structures were developed. Therefore, only a two-dimensional FE-discretization of the structure is necessary and the modelling effort can be reduced drastically. Optimization problems with thicknesses and number of layers as design variables can easily be solved, since the finite element can remain unchanged. Since for most stress analyses a two-dimensional model is used, the same model can be used for the thermal analysis when applying the new elements. Therefore, the effort for the integrated thermo-mechanical analysis is decreased and the transfer of the temperature distribution from the thermal to the stress model is very much simplified.

Three examples including an experimental verification test were analysed and compared with 3D analyses using MSC/NASTRAN. Under uniform loading QUADLLT already provided excellent results, whereas under non-uniform (concentrated) loading the quadratic element should be applied.

References

[1] Heemskerk JF, Delil AAM, Daniels DHW. Thermal conductivity of honeycomb sandwich panels for space application. Technical report, National Aerospace Laboratory NLR, The Netherlands, 1971.

[2] Chamis CC, Aiello RA, Murthy PLN. Composite sandwich thermostructural behaviour: Computational simulation. AIAA paper 86–0948, 1986. p. 370–81.

[3] Chin JH, Panczak TD, Fried L. Development of thermal modeling techniques for spacecraft. In: Lewis RW, Chin JH, Homsy GM, editors. Seventh International Conference on Numerical Methods in Thermal Problems, Standford, 1991. Numerical methods in thermal problems, vol. VII. Swansea: Pineridge Press; 1991. p. 1315–25.

[4] Rolfes R. Efficient thermal analysis of anisotropic composite plates using new finite elements. In: Füller J, Grüninger G, Schulte K, Bunsell AR, Massiah A, editors. Developments in the science and technology of composite materials, Fourth European Conference on Composite Materials (ECCM4), Stuttgart, 1990.

Barking (Engl.): Elsevier Science Publishers; 1990. p. 743–8.
[5] Rolfes R. Higher order theory and finite element for heat conduction in composites. In: Lewis RW, Chin JH, Homsy GM, editors. Seventh International Conference on Numerical Methods in Thermal Problems, Standford, 1991. Numerical methods in thermal problems, vol. VII. Swansea: Pineridge Press; 1991. p. 880–9.
[6] Warren AH, Arelt JE, Eskew WF, Rogers KM. Finite element-finite difference thermal/structural analysis of large space truss structures. AIAA paper 92-4763-CP, 1992.
[7] Surana KS, Kalim P. Isoparametric axisymmetric shell elements with temperature gradients for heat conduction. Comput Struct 1986;23(2):279–89.
[8] Surana KS, Phillips RK. Three dimensional curved shell finite elements for heat conduction. Comput Struct 1987; 25(5):775–85.
[9] Noor AK, Burton WS. Steady-state heat conduction in multilayered composite plates and shells. Comput Struct 1991;39(1/2):185–93.
[10] Rolfes R. Nonlinear transient thermal analysis of composite structures. In: Hirsch Ch, Zienkiewicz OC, Onate E, editors. Numerical methods in engineering'92, First European Conference on Numerical Methods in Engineering, Brussels, 1992. Amsterdam: Elsevier Science Publishers; 1992. p. 653–9.
[11] Rolfes R, Noack J, Taeschner M. High performance 3D-analysis of thermo-mechanically loaded composite structures. Compos Struct 1999;2(46):367–79.
[12] Rolfes R, Rohwer K. Integrated thermal and mechanical analysis of composite plates and shells. Compos Sci Technol 2000;60:2097–106.
[13] Argyris J, Tenek L, Öberg F. A multilayer composite triangular element for steady-state conduction/convection/radiation heat transfer in complex shells. Comput Meth Appl Mech Eng 1995;120:271–301.
[14] Surana KS, Orth NJ. Completely hierarchical p-version axisymmetric shell element for nonlinear heat conduction in laminated composites. Comput Struct 1993;46(5):777–89.
[15] Sipetov VS, Karpilovskii VS, Demchuk ON. Application of the finite element method to solve the stationary heat conduction problem of piecewise inhomogeneous systems. J Eng Phys 1989;55(6):1439–43.
[16] Bose A, Surana KS. Piecewise hierarchical p-version curved shell finite element for heat conduction in laminated composites. Comput Struct 1993;49(2):283–300.
[17] Noack J. Eine schichtweise Theorie und Numerik für Wärmeleitung in Hybridstrukturen, Dissertation, Shaker Verlag Aachen, 2000.
[18] Petersen D, Klein H, Schmidt K. DLR THERMEX-B test facility for cryogenic tank wall structures. AIAA 8th International Space Planes and Hypersonic Systems and Technologies Conference, Norfolk, VA, USA, 27–30 April 1998. p. 21–30.